Published in final edited form as:

*Neuroimage*. 2022 November 15; 262: 119555. doi:10.1016/j.neuroimage.2022.119555.

# Cerebral blood flow and cardiovascular risk effects on resting brain regional homogeneity

**Bhim M. Adhikari**[a], **L. Elliot Hong**[a], **Zhiwei Zhao**[b], **Danny J.J. Wang**[c], **Paul M. Thompson**[d], **Neda Jahanshad**[d], **Alyssa H. Zhu**[d], **Stefan Holiga**[e], **Jessica A. Turner**[f], **Theo G.M. van Erp**[g,h], **Vince D. Calhoun**[f,i], **Kathryn S. Hatch**[a], **Heather Bruce**[a], **Stephanie M. Hare**[a], **Joshua Chiappelli**[a], **Eric L. Goldwaser**[a], **Mark D. Kvarta**[a], **Yizhou Ma**[a], **Xiaoming Du**[a], **Thomas E. Nichols**[j], **Alan R. Shuldiner**[k], **Braxton D. Mitchell**[k], **Juergen Dukart**[l,m], **Shuo Chen**[a], **Peter Kochunov**[a,*]

[a]Maryland Psychiatric Research Center, Department of Psychiatry, University of Maryland School of Medicine, Baltimore, MD 21228

[b]University of Maryland, College Park, MD 20742



* Corresponding author at: Maryland Psychiatry Research Center, Department of Psychiatry, University of Maryland School of Medicine, Baltimore, MD 21228. pkochunov@som.umaryland.edu (P. Kochunov).

Credit authorship contribution statement

**B. M. Adhikari:** Formal analysis, Investigation, Methodology, Visualization, Writing – original draft, Writing – review and editing. **P. Kochunov, L. E. Hong**: Conceptualization, Research design and data acquisition, Funding acquisition and project administration, Writing – review and editing.

**S. Chen, Z. Zhao**: Data analysis, Methodology, Writing – review and editing

D. J. J. Wang, P. M. Thompson, N. Jahanshad, A. H. Zhu, J. A. Turner, T. G. M. van Erp, V. D. Calhoun, K. S. Hatch, H. Bruce, S. M. Hare, J. Chiappelli, E. L. Goldwaser, M. D. Kvarta, Y. Ma, X. Du, T. E. Nichols, A. R. Shuldiner, B. D. Mitchell: Writing – review and editing

**J. Dukart, S. Holiga:** Resources, Writing – review and editing

Data and code availability

Relevant data are made available in the manuscript. Imaging data and relevant codes will be made available upon request.

Competing Interests

LEH has received or plans to receive research funding or consulting fees on research projects from Mitsubishi, Your Energy Systems LLC, Neuralstem, Taisho, Heptares, Pfizer, Luye Pharma, Sound Pharma, Takeda, and Regeneron. None was involved in the design, analysis or outcomes of the study. NJ and PT received a research grant from Biogen, Inc., for research unrelated to this project. All other authors declare no conflicts of interest.

Credit authorship contribution statement

**Bhim M. Adhikari:** Data curation, Formal analysis, Investigation, Methodology, Visualization, Writing – original draft, Writing – review & editing. **L. Elliot Hong:** Conceptualization, Investigation, Funding acquisition, Project administration, Supervision, Writing – review & editing. **Zhiwei Zhao:** Formal analysis, Methodology, Writing – review & editing. **Danny J.J. Wang:** Writing – review & editing. **Paul M. Thompson:** Writing – review & editing. **Neda Jahanshad:** Writing – review & editing. **Alyssa H. Zhu:** Writing – review & editing. **Stefan Holiga:** Resources, Writing – review & editing. **Jessica A. Turner:** Writing – review & editing. **Theo G.M. van Erp:** Writing – review & editing. **Vince D. Calhoun:** Writing – review & editing. **Kathryn S. Hatch:** Writing – review & editing. **Heather Bruce:** Writing – review & editing. **Stephanie M. Hare:** Writing – review & editing. **Joshua Chiappelli:** Writing – review & editing. **Eric L. Goldwaser:** Writing – review & editing. **Mark D. Kvarta:** Writing – review & editing. **Yizhou Ma:** Writing – review & editing. **Xiaoming Du:** Writing – review & editing. **Thomas E. Nichols:** Writing – review & editing. **Alan R. Shuldiner:** Writing – review & editing. **Braxton D. Mitchell:** Writing – review & editing. **Juergen Dukart:** Resources, Writing – review & editing. **Shuo Chen:** Formal analysis, Methodology, Writing – review & editing. **Peter Kochunov:** Conceptualization, Investigation, Funding acquisition, Project administration, Supervision, Writing – review & editing.

Supplementary materials

Supplementary material associated with this article can be found, in the online version, at doi:10.1016/j.neuroimage.2022.119555.

[c]Laboratory of Functional MRI Technology, Mark and Mary Stevens Neuroimaging and Informatics Institute, Keck School of Medicine, University of Southern California, Los Angeles, CA 90007

[d]Imaging Genetics Center, Mark and Mary Stevens Neuroimaging and Informatics Institute, Keck School of Medicine, University of Southern California, Marina del Rey, CA 90292

[e]Roche Innovation Center Basel, Basel, BS

[f]Departments of Psychology and Neuroscience, Georgia State University, Atlanta, GA 30302

[g]Clinical Translational Neuroscience Laboratory, Department of Psychiatry and Human Behavior, School of Medicine, University of California, Irvine, CA 92697

[h]Center for the Neurobiology of Learning and Memory, University of California Irvine, Irvine, CA 92697

[i]Tri-Institutional Center for Translational Research in Neuroimaging and Data Science (TReNDS): (Georgia State University, Georgia Institute of Technology, and Emory University), Atlanta, GA 30302

[j]Nuffield Department of Population Health of the University of Oxford, Oxford, OX3 7LF, UK

[k]Department of Medicine, University of Maryland School of Medicine, Baltimore, MD 21201

[l]Institute of Neuroscience and Medicine - INM-7: Brain and Behaviour, Research Center Jülich, Wilhelm-Johnen-Straße, 52425 Jülich, Germany

[m]Institute of Systems Neuroscience, Medical Faculty, Heinrich Heine University Düsseldorf, 40225 Düsseldorf, Germany

## Abstract

Regional homogeneity (ReHo) is a measure of local functional brain connectivity that has been reported to be altered in a wide range of neuropsychiatric disorders. Computed from brain resting-state functional MRI time series, ReHo is also sensitive to fluctuations in cerebral blood flow (CBF) that in turn may be influenced by cerebrovascular health. We accessed cerebrovascular health with Framingham cardiovascular risk score (FCVRS). We hypothesize that ReHo signal may be influenced by regional CBF; and that these associations can be summarized as FCVRS→CBF→ReHo. We used three independent samples to test this hypothesis. A test-retest sample of $N = 30$ healthy volunteers was used for test-retest evaluation of CBF effects on ReHo. Amish Connectome Project (ACP) sample ($N = 204$, healthy individuals) was used to evaluate association between FCVRS and ReHo and testing if the association diminishes given CBF. The UKBB sample ($N = 6,285$, healthy participants) was used to replicate the effects of FCVRS on ReHo. We observed strong CBF→ReHo links ($p<2.5 \times 10^{-3}$) using a three-point longitudinal sample. In ACP sample, marginal and partial correlations analyses demonstrated that both CBF and FCVRS were significantly correlated with the whole-brain average ($p<10^{-6}$) and regional ReHo values, with the strongest correlations observed in frontal, parietal, and temporal areas. Yet, the association between ReHo and FCVRS became insignificant once the effect of CBF was accounted for. In contrast, CBF→ReHo remained significantly linked after adjusting for FCVRS and demographic covariates ($p<10^{-6}$). Analysis in $N = 6,285$ replicated the FCVRS→ReHo

effect ($p = 2.7 \times 10^{-27}$). In summary, ReHo alterations in health and neuropsychiatric illnesses may be partially driven by region-specific variability in CBF, which is, in turn, influenced by cardiovascular factors.

**Keywords**

Arterial-spin labeling; Correlation; Local functional connectivity; Multivariate mediation analysis; Resting state functional MRI

## Introduction

Regional homogeneity (ReHo) is an index of synchronization between the blood oxygenation level dependent (BOLD) time series of a voxel and its nearest neighbors in resting state functional MRI (rsfMRI) time series data (Biswal et al., 1995; Fox et al., 2007). This measure is speculated to be informative of local – rather than long-distance – resting-state functional connectivity (rsFC) (Wang et al., 2011; Zang et al., 2004). It is considered a promising biomarker in neuropsychiatric illnesses and has been linked to symptoms, cognition and other clinical features in schizophrenia, depression, Alzheimer's disease, stroke, and other illnesses (Chen et al., 2013; Jiang and Zuo, 2016; Li et al., 2017; Qiu et al., 2011; Zuo et al., 2013). The findings of lower ReHo signal in patients vs. controls is commonly interpreted as evidence for connectivity deficits or aberrant synchronization (Han et al., 2011; Iwabuchi et al., 2015; Jiang et al., 2015; Qiu et al., 2011; Zhang et al., 2012). However, we lack a clear mechanistic explanation for these findings, due to limited empirical data available to support the assumption that ReHo is driven by local neural connectivity differences (Gao et al., 2020; Zhu et al., 2015).

ReHo has been studied and validated in laboratory animal models in which ReHo findings have been demonstrated to be robust and replicable (Dong et al., 2020; Li et al., 2018; Rao et al., 2017, 2015). For example, in a stress-based rat model of depression, widespread ReHo alterations were observed in cortical regions in stressed animals and these changes were reversed or attenuated by pharmacological interventions (Dong et al., 2020; Li et al., 2018). Changes in regional ReHo values were also observed in cortical and subcortical areas under different anesthesia medications in laboratory rodents (Wu et al., 2017). Ketamine administration in rhesus monkeys increased ReHo in the nucleus accumbens, caudate nucleus, and hippocampus but decreased ReHo in the prefrontal cortex (Rao et al., 2017). Similar to human studies, most of the ReHo changes in animal disease models or pharmacological challenges have been interpreted as changes in local brain functional states or resting local intrinsic synchrony (Rao et al., 2017; Wu et al., 2017). However, like most human studies, these findings provide insufficient evidence for exclusively linking ReHo changes to synchronized local neural activity.

Pharmacological interventions in laboratory animals, including ketamine and anesthetic agents, are known to induce significant changes in cerebral blood flow (CBF), blood pressure, and pulse pressure (Cavazzuti et al., 1987; Hassoun et al., 2003; Sugita et al., 2018; Temma et al., 2008). When neighboring voxels are examined for temporal correlations, any signals with shared local temporal fluctuations may contribute to the correlation strength.

Synchronized neuronal firing, e.g., functional connectivity, may explain the synchronized BOLD signals. However, temporal synchronization can also be produced by fluctuations in the regional CBF as the neighboring voxels are likely to share the same blood supply, resulting in increased or decreased ReHo coefficients beyond that produced by neuronal synchronization. If true, this should not be interpreted as the 'local connectivity' as it would result from a shared vascular or systemic cause of shared events among neighboring voxels rather than a neuronal cause.

ReHo signals may still reflect the underlying neural rather than vascular mechanism, when regional CBF changes follow the level of neural activity in neighboring voxels. This is possible because in healthy conditions regional CBF is rigorously regulated to equalize the metabolic demand and supply for neural activities (Meng et al., 2015). One way to disentangle the neuronal vs. vascular relationship is to look at the roles of non-neural vascular contributions. CBF normally takes up to a ~15% proportion of the cardiovascular output (Williams and Leggett, 1989), but cardiovascular risk factors can alter the temporal trends and magnitude of the CBF response to neuronal activity both globally and regionally (Meng et al., 2015). If system-level cardiovascular effects can be shown to significantly contribute to ReHo directly or through its effect on CBF, it gives weight to the argument that ReHo is not exclusively a measure of local neuronal functional connectivity.

We used a recognized index of cardiovascular disease risk (CVDR) factors, the FCVRS (D'Agostino et al., 2008), to test the hypotheses that, first, FCVRS may impact ReHo in a regional specific pathway (FCVRS → ReHo regions), and second, this effect is mediated by CBF, also in a regional specific pathway (FCVRS → CBF region → ReHo region). Further, the regional effect can be isoregional (i.e., ReHo is affected by CBF from the same region) or hetero-regional (e.g., ReHo of a region(s) is affected by CBF from other regions, not just the same region(s)). We performed exploratory multivariate mediation analysis to parse the total effect of FCVRS on regional ReHo into the direct FCVRS effect on ReHo (no CBF involved) and mediated pathways whereby FCVRS affects ReHo through iso or hetero-CBF regional changes. This approach adds the necessary spatial information to the traditional mediation pathway analysis by considering the likely three-dimensional mediations.

We addressed these questions in a sample of adult participants with no history of psychiatric illnesses from the Amish Connectome Project (ACP), which included members of the Old Order Amish/Mennonite (OOA/M) population. Compared to the general United States population, at the population level the OOA/M have a more homogeneous rural lifestyle and have low rates of substance misuse (Fuchs et al., 1990; Nugent et al., 2014). Together this may allow identification of potential cerebral blood supply effects on ReHo with reduced confounds. We addressed the replicability and generalizability of our findings by repeating the FCVRS and ReHo analysis in a large and inclusive sample of healthy, non-psychiatric participants in the UK Biobank (UKBB). A longitudinal dataset acquired at three different time points (Neuroimaging Center, University Medical Center Groningen (UMCG), Netherlands) were used and analyses were performed using whole-brain average signals to address the replicability and generalizability of the CBF effect on the ReHo measures.

## Materials and methods

### Study participants

*N* = 30 (age: 25 ± 5 years [mean ± standard deviation]; 7 males/23 females) participated in the test-retest study after providing written informed consent. The health status was defined by the absence of any active or chronic disease or positive signs on a complete physical examination including vital signs, 12-lead electrocardiogram, hematology, blood chemistry, serology and urinalysis (Holiga et al., 2018). The study was carried out according to local regulations and the International Council for Harmonization of Technical Requirements for Pharmaceuticals for Human Use guidelines at a single center (UMCG, Netherlands). Subjects were scanned at three different time points; a screening period of 28 days (15±3 days before the baseline Visit 1, called Visit 0) preceded the study assessment period and subsequently, two study visits (Visit 1 and Visit 2) were performed fourteen days apart.

*N* = 204 OOA/M participants (94 males/110 females, age: 39.3 ± 16.9 years, mean ± s.d.) with no history of psychiatric diagnoses from the ACP (https://www.humanconnectome.org/study/amish-connectome-project). This cohort shares a similar rural upbringing and lifestyle that includes the same level of basic school education, diet, and occupations, and virtually no illicit substance use and offers a population-level reduction in environmental heterogeneity that may confound cardiovascular and cerebral blood flow measures. Individuals having a lifetime diagnosis of psychiatric disorders were excluded in this analysis to avoid confounded effects of psychiatric illnesses. Other exclusion criteria included major medical and neurological conditions that might affect gross brain structures - such as developmental disability, head trauma, seizure, stroke, or transient ischemic attack. All participants provided written informed consent on forms approved by the Institutional Review Board of University of Maryland Baltimore.

A UKBB sample of 6285 participants (3384 males/ 2901 females, age: 56.6 ± 7.5 years, mean ± s.d.) who were selected from ~17,000 subjects with imaging data provided by the first UKBB release. These subjects were selected to be free from any neuropsychiatric or metabolic disorder such as types 1 and 2 diabetes, hypo- or hyperthyroidism, brain trauma and other ICD-10 diagnostic status and were included for replication of the findings related to FCVRS and ReHo measurements.

### Arterial-spin labeling data acquisition and processing

The ACP sample had arterial-spin labeling (ASL) data, but the UKBB sample had no ASL data. ASL data for ACP sample were acquired on a 3 T Siemens Prisma scanner with 64 channels, using three-dimensional pseudo-continuous ASL (pCASL) with background suppressed gradient and spin-echo sequence consisting of 13 pairs of labeled and control scans. The acquisition parameters were spatial resolution = 2.5 mm × 2.5 mm × 2.6 mm, matrix size = 96 × 96 with 58 axial slices, repetition time/echo time (TR/TE) = 4000/37 ms, flip angle = 120°, field of view (FoV) read = 220 mm, FoV phase = 100%, post-label delay = 1700 ms, labeling duration = 1650 ms. Total scan time was approximately 10 min. A 3D $T_1$-weighted image was acquired for anatomical reference, as well as gray and white matter tissue segmentation, with the following parameters: TR = 2400 ms, TE = 2.22 ms,

inversion time = 1000 ms, flip angle = 8°, matrix = 300 × 320, slices per slab = 208, 0.8 mm × 0.8 mm spatial resolution with slice thickness = 0.80 mm. A volume of $M_0$ image was also acquired without background suppression to normalize the control-label difference for CBF quantification. To suppress effects of noise, the $M_0$ image was smoothed with a 5 mm Gaussian-kernel, as recommended in a recent ASL white paper (Alsop et al., 2015).

ASL dataset at Neuroimaging Center, UMCG, Netherlands was acquired using a 3 T clinical scanner (Intera, Philips Healthcare, Best, Netherlands) with a 32-channel head coil. For CBF computation 60 pairs of labeled and control images with 17 axial slices, 7 mm slice thickness and no gap covering the whole brain were collected using a pCASL sequence (*TR* = 4000 ms; *TE* = 14 ms, *FA* = 90°; labeling duration = 1650 ms; post-labeling delay = 1600 ms; labeling gap = 2 cm; in-plane resolution = 3 × 3 $mm^2$). A 2D single-shot echo-planar imaging (EPI) readout with fat suppression was used. Additionally, a separate proton density image ($M_0$) was collected to obtain voxel-wise intensity of fully relaxed blood spins.

CBF data analysis was performed with the FSL software package; perfusion was estimated by using a standard single compartment ASL model; partial volume effects correction was performed with a spatially regularized method (Chappell et al., 2011). Spatial regularization, motion correction and partial volume corrections were performed in FSL v6.0.1. The high-resolution structural image provides partial volume estimates (PVE) for the different tissue types (gray matter (GM), white matter (WM), and cerebrospinal fluid). The high-resolution PVE images obtained from a structural image were then converted to the ASL image space using a transformation matrix from the structural space to the ASL native image space. Partial volume corrected CBF maps were used to extract the regional CBF signals from parcellated GM (both cortical and subcortical) and WM structures, separately for both hemispheres, defined in the brain template ‘Everything Parcellation Map in Eve Space’ atlas- also called the ‘EvePM’ atlas (Lim et al., 2013); we refer to this as the JHU-MNI atlas from now on. EvePM atlas allows automated segmentation of gray matter and white matter structures with hemispheric differentiation. This atlas combined a deep gray matter parcellation map derived from a single-subject quantitative susceptibility map with white matter parcellation map into an MNI coordinate and included 107 ROIs. The extracted signals were used in the statistical analyses.

### Resting state functional MRI (rsfMRI) data acquisition, processing, and analyses

All ACP participants underwent rsfMRI data acquisition that consisted of two runs. Oblique axial acquisitions alternated between phase encoding in the anterior-to-posterior (AP) and posterior-to-anterior (PA) directions within a single run. Separate single-band reference images, acquired for phase encoding in AP and PA directions, were used for spatial distortion correction. RsfMRI data were acquired using the following parameters: TR = 780 ms, TE = 34.4 ms, spatial resolution of 2-mm isotropic voxels, matrix size = 104 × 104 with 72 axial slices, number of volumes = 420, flip angle = 52°, multi-band acceleration factor = 8, and bandwidth = 2186 Hz/pixel.

UKBB rsfMRI data were acquired on 3 T Siemens Skyra scanners with the standard Siemens 32-channel receive head coil using the following parameters: TR = 735 ms, TE = 39 ms, spatial resolution of 2.4-mm isotropic voxels, matrix size = 88 × 88 with 64 axial

slices, number of volumes = 490, flip angle = 52°, and multi-band acceleration factor = 8. A separate single-band reference image was acquired and used as the reference scan for head motion correction and alignment to other modalities (Alfaro-Almagro et al., 2018).

RsfMRI dataset at UMCG were acquired on a 3 T clinical scanner using a 32-channel head coil. 244 vol of BOLD effect sensitive images covering the whole brain were acquired using a gradient-echo EPI sequence (TR = 2000 ms, TE = 30 ms; FA = 90°; 39 axial slices with 1 mm gap, nominal in-plane resolution $3 \times 3\ mm^2$ ; slice thickness at 3 mm) (Holiga et al., 2018).

The resting state analysis workflow developed by the Enhancing Neuro Imaging Genetics through Meta-Analysis (ENIGMA) consortium was used to process the rsfMRI data; processing steps have been described in full detail in prior publications (Adhikari et al., 2018a, 2018b). The analysis workflow uses Marchenko-Pastur principal component analysis denoising (Veraart et al., 2016) to improve signal-to noise ratio (SNR)/temporal SNR of the time series data. In this workflow, a transformation is computed registering the base volume to the ENIGMA EPI template, which is used as a common anatomical spatial reference frame for registration purposes. This step was followed by 3D deconvolution of methodological covariates, and regression of the global signal (Adhikari et al., 2019). Each functional volume was registered to the volume with the minimum outlier fraction for head motion correction, where each transformation was concatenated with the transformation to standard space, to avoid unnecessary interpolation. We removed the effects of the following nuisance variables by using them as covariates using multiple linear regression analysis: the six (three rotations and three translations) motion parameter and their temporal derivatives, and time courses from the local white matter and cerebrospinal fluid from lateral ventricles. Motion was estimated as the magnitude of displacement from one time point to the next including neighboring time points and outlier voxels fraction (> 0.1). Time points with excessive motion (>0.2 mm) were excluded from further statistical analysis. Images were spatially normalized to the ENIGMA EPI template in MNI standard space for group analysis and then to JHU-MNI atlas template in order to extract measures from ROIs based on this template. The pre-processed data was then used for ReHo calculations.

## ReHo analysis

ReHo was designed to investigate changes in local spontaneous brain activity by performing a nearest neighbor analysis of similarity of the BOLD time-series and assigning a score, called Kendall's coefficient of concordance (KCC) (Zang et al., 2004) per voxel. The KCC score is calculated per voxel based on signals from neighboring voxels as: $W = \frac{\sum(R_i^2) - nR^2}{\frac{1}{12}K^2(n^3 - n)}$.

Here, $W$ is the KCC among given voxels, ranging from 0 to 1; $R_i$ is the sum rank of the $i^{th}$ time point; $R = ((n + 1)K)/2$ is the mean of the $R_i$'s; $K$ is the number of time series within a measured cluster ($K$ is set to be 7, 19, or 27), and $n$ is the number of ranks ($n$ = number of volumes) (Zang et al., 2004). $K$ was set to be 27, which is appropriate for covering all directions in 3D space and to optimize the trade-off between mitigation of partial volume effects and generation of Gaussian random fields (Jiang and Zuo, 2016). For each subject,

the ReHo map was computed in three-dimensional volumetric space using the MATLAB function '*y_reho.m*' available in the *DPABI_V3.0_171210* package.

To extract global and regional ReHo and CBF signals, we selected the JHU-MNI atlas that includes both GM and WM brain structures from both hemispheres. Global signals, based on this atlas, included the contribution from these both GM and WM regions. Also, time courses from the local WM and CSF from the lateral ventricles were modeled using multiple linear regression analysis, and then removed as regressors of no interest during data processing. Using these measures, we performed correlation analyses between ReHo signals with CBF signals and cardiovascular disease risk score and also performed the mediation analysis. For the UKBB sample, we extracted the global and average regional ReHo signals for the same ROIs. We then performed correlation analysis between these signals and the cardiovascular disease risk score.

## FCVRS

Cardiovascular disease risk was assessed using the FCVRS. The FCVRS summarizes the estimated contribution of risks as a FCVRS value from systolic blood pressure, blood plasma lipid measures including total cholesterol and high-density lipoprotein (HDL) cholesterol, and other factors such as diabetes, age, sex, and smoking status (Haight et al., 2015). The original FCVRS study provided the% risk corresponding to the actual score side by side for clinical use (D'Agostino et al., 2008). For the ACP sample, we analyzed the relationships between FCVRS, CBF and ReHo signals. The FCVRS from UKBB participants were used to investigate the relationship with the ReHo signals.

All analyses were performed after regressing the effects of age to address the potential collinearity in the Framingham cardiovascular risk scores and aging-related decline in CBF. We had no specific hypotheses regarding sex-related differences and therefore all analyses were also corrected for sex of the participants.

## Exploratory mediation analyses

Establishing causal links using cross-sectional data is challenging. We used the causal discovery analysis to demonstrate that ReHo and CBF are non-independent contrast mechanism that share a common risk factor (Glymour et al., 2019). The mediation analysis conducted in this study represents the test of the main hypothesis FCVRS → CBF → ReHo rather than establishing a causative biological mechanism (Serang et al., 2017).

We first performed two simpler levels of mediation analyses to explore the data. In this analysis, we first calculated the whole-brain average CBF and ReHo data and performed the exploratory mediation analysis, based on whole-brain average signals to test whether whole-brain average CBF would significantly mediate the relationship between FCVRS and whole-brain average ReHo. Second, we performed an isoregional mediation analysis by arbitrarily restricting the CBF and ReHo signals to the same region, i.e., testing whether CBF from each region would significantly mediate the FCVRS effect on ReHo from the same region. For the primary analysis, we developed a mediation model with multiple mediators (i.e., CBF measures from one or many regions) and multiple outcomes (i.e., ReHo measures from one or many same and/or different regions), while age and sex were

considered as covariates of no interest. The commonly used assumptions (e.g., sequential ignorability) were used for identification for the mediation model (Chen et al., 2018). Here, we focused on a method we called hetero-regional multivariate mediation analysis, which refers to FCVRS → CBF in a given cluster(s) → ReHo in another cluster(s), where FCVRS affects CBF and then influences ReHo through CBF. The mediation effect can be interpreted as follows: FCVRS can influence ReHo of certain territories via certain CBF territories, where regions for CBF and regions for ReHo can be entirely separated, partially overlapped, or totally overlapped. We extracted mediation bi-clusters using tailored adaptive dense graph discovery algorithms (Jahanshad et al., 2010; Wu et al., 2020). A mediation bi-cluster includes a set of CBF regions and the corresponding cluster ReHo regions, which reflects FCVRS influencing ReHo regions via the CBF regions within the bi-cluster.

Next, we estimated the mediation effect for each mediation bi-cluster by decomposing the total effect of FCVRS on ReHo into a natural direct effect (NDE) and a natural indirect effect (NIE). The NDE was tested by assessing the effect of FCVRS on a ReHo region while controlling the effects of all related CBF regions and covariates. The standardized mediation effect was used to calculate NIE (Chen et al., 2018). When multivariate mediators were selected, dimension reduction method was used to translate multivariate mediators into a few orthogonal components for estimating NDE and NIE (Chen et al., 2018). Permutation tests were performed to control the family-wise error rate of cluster-wise inference (Nichols and Holmes, 2002). We further explored whether specific measure(s) within the FCVRS had a predominant effect on CBF and/or ReHo. For statistical inference, the alpha level of 0.05 was used, while the corrected threshold for multiple comparison methods (e.g., false discovery rate and family-wise error rate controls) was also 0.05. The key mathematical formulae for this mediation analysis procedure were detailed in supplementary document.

We expanded this study by including a dataset acquired at three different time-points to establish the CBF→ ReHo relationship using whole-brain average CBF and ReHo signals. In addition, we also performed the partial correlation analyses using the FCVRS, CBF and ReHo measures (results were detailed in the supplementary document). Supplementary Fig. S1 summarizes the datasets, measures and the tests used to address different parts of the research hypothesis.

## Results

### ReHo and CBF whole brain distribution maps

Whole brain distributions of resting ReHo and resting CBF are shown in Fig. 1. By visual examination, bilateral frontal areas as well as the insula, parieto-occipital areas, temporal areas and cingulate gyrus showed greater CBF and ReHo signals. White matter regions exhibited lower ReHo and CBF signals, compared to other brain areas. Bilateral cerebellum showed lower CBF, but not lower ReHo signals, whereas bilateral fronto-orbital gyrus showed comparatively greater CBF signals, but lower ReHo signals. Overall, there was a similar visual appearance in the ReHo and CBF maps ($N = 204$), including the contrast between white and gray matter (Fig. 1).

### ReHo and CBF relationship

The test-retest dataset was used to establish a link between CBF and ReHo. The whole-brain average CBF signals drove the whole-brain average regional homogeneity signals ($p \leq 0.0028$, Cohen's $f^2 > 0.46$, within/between visits). The regression models (ReHo ~ CBF + covariates) showed the statistically significant positive association in all visits and CBF signals drive the ReHo signals. Changes in CBF led to changes in ReHo signals from visit to visit. In addition, these CBF and ReHo measures were reproduceable. The full results are provided in Table S1 and Fig. S3 and S4, see supplement.

We replicate the correlation between the whole-brain average ReHo and CBF signals were significantly and positively correlated ($r = 0.46$, $p = 3.1 \times 10^{-11}$) in ACP subjects and this correlation remained significant after correcting for age and sex ($r = 0.41$, $p = 8.5 \times 10^{-9}$) (Fig. 2A). The ReHo and CBF signals of many regions likewise showed positive correlations, where the correlation coefficients in 42 out of 107 regions survived multiple comparisons correction (Bonferroni correction, $p* < 0.05$). The significant correlation values varied from 0.25 ($p = 4.0 \times 10^{-4}$) to 0.41 ($p = 5.4 \times 10^{-9}$) (Fig. 3A), no negative correlation was found in any region. The significantly correlated regions include bilateral frontal, temporal, parietal (superior) and fronto-orbital regions; thalamus and insula, but most of the subcortical and white-matter regions showed statistically insignificant correlation between regional CBF and ReHo signals. Regional correlation values are in supplementary Table S2 (A).

### FCVRS contributions to CBF

The FCVRS varied from −8 to 17 (mean: 2.8 ± 5.2) for ACP participants aged 18–76 years (mean: 39.3 ± 16.9 years). FCVRS was significantly and negatively correlated with the whole-brain average CBF signals ($r = -0.41$, $p = 9.1 \times 10^{-9}$) after correcting for age and sex (Fig. 2B). The regional CBF signals from many regions likewise were negatively correlated with FCVRS: 59 out of 107 regions survived Bonferroni multiple comparisons correction ($p* < 0.05$). The significant regional correlation values ranged from −0.25 ($p = 4.4 \times 10^{-4}$) to $r = -0.47$ ($p = 7.7 \times 10^{-12}$), mainly in bilateral frontal, parietal, occipital, fronto-orbital, and insular regions and right pre/postcentral, caudate, and midline structures in midbrain, pons and cingulum. Most of the white matter and subcortical regions did not show statistically significant correlation between these signals (Fig. 3B). Region-by-region correlation values are in supplementary Table S2 (B).

### FCVRS contributions to REHO

FCVRS was negatively correlated with the whole-brain average ReHo signals after correcting for age and sex ($r = -0.31$, $p = 1.4 \times 10^{-5}$) (Fig. 2C). Regionally, FCVRS showed negative correlation with ReHo in 12 out of 107 regions after Bonferroni correction (values ranged from −0.25 ($p = 4.6 \times 10^{-4}$) to $r = -0.40$ ($p = 1.8 \times 10^{-8}$) (Fig. 3C). The strongest correlations were observed for bilateral frontal, insular and medial fronto-orbital regions. Mostly sub-cortical and white-matter regions were statistically insignificant. The region-by-region correlation coefficients are shown in supplementary Table S2 (C).

Overall, the correlation coefficients computed between FCVRS and CBF and those computed between FCVRS and ReHo are themselves also significantly correlated across regions ($r = 0.57$, $p = 2.2 \times 10^{-10}$ ; Fig. S2A), suggesting that the regional distributions of the CBF and the ReHo signals showed a similar pattern of negative correlation with the FCVRS.

## Replications in the UKBB

Our replication test was limited to the FCVRS and ReHo relationships as no ASL data was available to the UKBB sample. The UKBB participants were older: 40 −70 years (56.6 ± 7.5 years), so their FCVRS was much higher at 10.2 ± 3.5. Despite the large differences in FCVRS, FCVRS in UKBB was significantly and negatively correlated with the whole-brain average ReHo ($r = -0.15$, $p = 2.7 \times 10^{-27}$) after correcting for age and sex (Fig. 2D). The regional ReHo signals also showed significant negative correlations with the FCVRS in 95 out of 107 regions after Bonferroni correction, with frontal areas again demonstrating the strongest effects (Fig. 3D; values are provided in supplementary Table S2 (D)). This is consistent with the ACP data where higher FCVRS scores were associated with lower ReHo signals. Furthermore, the correlation coefficients between FCVRS and ReHo themselves showed a strong correlation between the ACP and UKBB across regions ($r = 0.45$, $p = 1.1 \times 10^{-6}$ , Fig. S2B).

## Exploratory mediation analyses

Based on the mediation analyses performed to examine the potential mediators of the possible mediation process, three conditional independence tests provided: FCVRS → CBF|ReHo, correlation = −0.3095, $p<0.0001$; FCVRS → ReHo|CBF, correlation = −0.1548, $p = 0.03441$; and ReHo → CBF|FCVRS, correlation = 0.3852, $p<0.0001$. It then becomes clear that the only conditional independence after multiple testing correction is ReHo independent of FCVRS given CBF, which breaks the mediation pathways e.g., CBF → FCVRS → ReHo. Then, the collider does not hold because FCVRS and ReHo marginally correlated. Also, biologically CBF directly causes FCVRS changes is biologically less intuitive. Thus, the most likely causal pathway for mediation analyses was FCVRS → CBF → ReHo, which was *a prior* hypothesis. Fig. S7 summarizes the mediation analysis schemes.

## Whole-brain average mediation analysis

The mediation analysis performed using whole-brain average signal showed that the FCVRS effect on average ReHo was significantly mediated by average CBF. The mediation proportion effect was 51.9% ($p<0.0001$) based on the whole-brain averages (Fig. 4A).

## Whole-brain isoregional mediation analysis

We examined the mediation effect of CBF in each region on the direct FCVRS effect on ReHo from the same region. The effect size values were computed region-by-region using mediation proportion (i.e., using component analysis for CBF, 1 component with ~80% variance explained). The mediation effects were found to be significant for 65 regions with false discovery rate (FDR, $q<0.05$) among the 107 regions. The brain-wide distribution of the region-by-region mediation effects is displayed in Fig. 4B (detailed in supplementary

Table 3). The top ranked 18 of the 65 regions demonstrating a very strong mediation effect (FDR, $q<10^{-8}$) included bilateral superior parietal, inferior frontal, orbito-frontal, temporal areas, and hippocampus, parahippocampal, thalamus and putamen.

## Hetero-regional mediation analysis

CBF from one region is unlikely to mediate FCVRS effects on ReHo only in the same region. Thus, we carried out the primary multivariate mediation analysis using all potential combinatorial effects among 107 regional CBF measures as mediators and 107 regional ReHo measurements as the outcomes, to test for the patterns of mediation effects of FCVRS → one or any set of CBF regions → any one or any set of ReHo regions. The search heuristic was based on the null hypothesis that the probability of several CBF regions significantly mediating the effect of FCVRS on a set of ReHo regions converges to zero. The *p*-value matrix of this mediation analysis is shown in Fig. 5A. A systematic mediation pattern cluster (Fig. 5B), assessed using cluster-wise inference, remained significant after correcting for the family-wise error rate (FWER, $p = 0.001$). This mediation cluster included 45 regions and showed that regional CBF of each of these 45 regions significantly mediated the relationship between FCVRS and a cluster of 43 regional ReHo signals (Fig. 5B). The CBF cluster consisted of the bilateral frontal, temporal, occipital, orbito-frontal, parahippocampal and insular areas; and also, the left amygdala, right postcentral and right precuneus areas (Fig. 5C (i)). The ReHo cluster consisted of bilateral temporal, orbito-frontal, hippocampal, parahippocampal, superior parietal and inferior frontal areas, putamen, thalamus, cerebellum and cingulum, and right middle frontal and temporal regions and left pre/post-central and precuneus areas Fig. 5C (ii)). The mediation effect size values are in supplementary Table 4 (excel file). The CBF and ReHo territories only partially overlapped in 26 regions including bilateral inferior frontal, superior parietal, superior and inferior temporal, lateral and medial fronto-orbital areas (Fig. 5D). Based on the mediation bi-cluster, we calculated the direct effect and indirect effect for each ReHo region by the orthogonal components of the multivariate mediators (i.e., 45 CBF regions). We found that ~82% of the variance of the mediators in the bi-cluster was explained by one mediating factor. For the indirect effect calculation based on this mediating factor for all 43 ReHo regions, the mean standardized mediation effect size (i.e., partial correlation product) ± standard deviation is medium, −0.105 ± 0. 012.

We also explored whether specific individual measure(s) within the FCVRS had a predominant effect on CBF and/or ReHo. Briefly, significant mediation effects were found separately for age, total cholesterol and systolic blood pressure when each was considered as an individual factor for mediation analyses, suggesting that the mediation effects were not driven by a single measure. Most of the regions involved in the mediation effects in these analyses were the subsets of the regions that were significant in the mediation analysis using FCVRS. However, no significant mediation patterns were found for the other remaining components within the FCVRS measure.

## Discussion

This study demonstrated strong linkage between CBF and ReHo signal on both global and regional levels and showed that variance in both signals is influenced by cardiovascular risk factors. We showed that the impact of cardiovascular risks quantified FCVRS can be summarized as FCVRS → CBF → ReHo. That is higher FCVRS is associated with lower CBF, especially in the frontal, temporal and parietal areas, which in turn reduces both global and regional ReHo. The multivariate mediation analysis identified a systematic pattern involving 45 CBF regions that significantly influenced 43 ReHo regions. The analyses indicated that the regional ReHo variance due to FCVRS were due to regional CBF changes. While the underlying mechanistic associations among FCVRS, CBF and ReHo are complex, this study suggests caution in interpreting ReHo-related functional and disease effects as evidence for altered local connectivity. Instead, individual differences in cerebrovascular health play a significant role and must be included in the interpretation of the findings.

Abnormal ReHo signals are commonly reported in neuropsychiatric disorders (An et al., 2013; Dai et al., 2012; Fang et al., 2021; Qiu et al., 2011). For instance, patients imaged during an acute psychotic episode exhibited increased ReHo in the medial/lateral prefrontal cortex, anterior insula, and putamen and these findings were interpreted as evidence for increased local connectivity (Wang et al., 2018, 2016; Xiao et al., 2017; Xu et al., 2015). Similarly, higher ReHo values were reported in the left superior frontal gyrus and left inferior temporal gyrus in early-onset Parkinson's disease (Sheng et al., 2016), left anterior cingulum cortex in major depressive disorder patients (Song et al., 2022), right superior temporal gyrus and bilateral hippocampus, parahippocampus, fusiform gyrus and cerebellum in patients with obsessive–compulsive disorder (Yan et al., 2022), in right superior and inferior frontal gyrus in depressive patients compared to non-depressive patients (Fang et al., 2021). The lower ReHo signal in frontal and temporal lobes in patients with schizophrenia, Alzheimer's disease, and mild cognitive impairment were associated with a lower working memory performance and other cognitive abilities (Han et al., 2011; Zhang et al., 2012) and lower ReHo in the right putamen in early-onset PD compared to late-onset (Sheng et al., 2016). Conversely, increased synchronized local activity in the medial prefrontal cortex could be pursued as a surrogate measure for treatment monitoring and may possibly be considered a marker for depression (Iwabuchi et al., 2015). While most studies have appropriately interpreted these findings only as possibly related to local synchronized neural activities, to our knowledge, no studies have raised the question or tested whether cerebral blood flow, and overall cardiovascular risk factors, may also be contributors to the ReHo signals.

Findings in this study would suggest that ReHo-related group differences in neuropsychiatric conditions may in part be related to systemic cerebrovascular differences and risk factors. Cardiovascular risk factors such as hypertension, aging, and higher cholesterol levels promote arterial stiffness, damages in small cerebral blood vessels, and formation of atherosclerotic plaques, causing altered dynamics in blood flow through stenotic cerebral blood vessels (Carmichael, 2014). Subjects with neuropsychiatric disorders may have higher cardiovascular risk (Giordano et al., 2007; Luchsinger and Gustafson, 2009; Timothy et al., 2003) and accelerated aging (Bersani et al., 2019; Viron and Stern,

2010; Wertz et al., 2021) and these differences may be difficult to fully control or remove in many ReHo studies. Moreover, pharmacological treatments for neuropsychiatric illnesses have side effects that adversely affect cardiovascular profiles and may be associated with metabolic syndrome (Casey et al., 2004; del Valle et al., 2006) that may alter brain functions (Beauchet et al., 2013; Gonzales et al., 2017; Hoogenboom et al., 2014; Roberts et al., 2014; Wang et al., 2015). As cardiovascular factors, most of them unlikely to be neuronal in origin, already show notable effects on ReHo in healthy, non-psychiatric controls in our study, it is likely that higher cardiovascular and metabolic risks in many neuropsychiatric illnesses may even more strongly impact the ReHo measures. ReHo measures can also be affected by the magnitudes of fMRI fluctuations (and SNR) and the size of the examined region, which may lead to have smaller ReHo values for subcortical regions and hence, the insignificant CBF-ReHo coupling as observed in these regions in our study.

Our findings replicate the outcome of the research that demonstrated that higher FCVRS were associated with lower cerebral metabolic rate of glucose in medial frontal, orbitofrontal, and inferior frontal/insular areas (Kuczynski et al., 2009a, 2009b). Furthermore, measures derived from the resting fMRI are expected to be correlated with CBF (Li et al., 2012; Zhu et al., 2017) and likewise ReHo measurements have been linked to CBF and/or perfusion imaging (Alsop et al., 2015; Detre et al., 1992; Williams et al., 1992). We replicated the negative trends between ReHo and FCVRS in the independent UKBB sample. The overall strength of the correlation between ReHo and FCVRS were lower in UKBB population ($r$=−0.15 vs. −0.31, $z$ = 4.0, $p$ = 0.0001). This could be driven by methodological differences between two datasets. The ACP dataset was collected using longer acquisition time (~22 min vs. 6 min with similar repetition times 780 ms vs. 735 ms for ACP and UKBB, respectively) and at higher spatial resolution (isotropic 2 mm vs. isotropic 2.4 mm voxel). The higher temporal signal to noise ratio of the ACP sample may have led to more stable estimates of the global and regional ReHo values.

While the ReHo measurements shared variance with CBF, this relationship is both complex and region-specific. The global and isoregional CBF was a robust mediator of the FCVRS effect on the global and isoregional ReHo signal. However, one-to-one analyses have overlooked the complex regional nature CBF→ReHo relationship. The mediation analysis was used to test if CBF significantly mediated the isoregional FCVRS effect on ReHo. It showed small (Fig. 4B) but significant ($q$<0.05) effect sizes across frontal, parietal, temporal areas and subcortical structures. We used a multivariate mediation analysis that treated regional CBF and ReHo patterns as two vectors and probed all-to-all associations. This analysis demonstrated that the FCVRS effects on regional ReHo signals were exerted by both the direct and mediated pathways.

The frontal lobe areas (inferior, middle and superior frontal gyri) showed the strongest correlations between the CBF and ReHo signals. They also showed the largest negative contrast with the FCVRS. Many of the frontal, parietal, temporal and deep gray matter brain regions that were identified as the key mediators are the areas associated with higher-order information processing and act as the key nodes in the functional networks (Briggs et al., 2019; Petrides, 2007; Ullsperger and von Cramon, 2001). We identified global and region CBF signals as the significant mediators of FCVRS to ReHo pathway, likely other factors

such as cerebrovascular reactivity (also relating to CBF) may also mediate this relationship. The regional mediation map follows the blood supply patterns provided by carotid versus vertebral-basilar circulations, replicating the cerebrovascular illness risk patterns for stroke, cerebral ischemia and vascular dementia (Albrecht et al., 2020; Blair et al., 2020; Dounavi et al., 2021; Knight et al., 2021). The high metabolic demands of the frontal and parietal areas may make them more susceptible to the cardiovascular factors. In agreement, ReHo signal from these areas also showed higher correlations with cardiovascular risks, through CBF pathway.

The ENIGMA-pipeline used for calculation of rsfMRI-ReHo signal includes the global signal regression (GSR). The global signal in rsfMRI data is associated with head motion, respiration and cardiac rhythms (Birn et al., 2006; Power et al., 2014). GSR is a necessary pre-processing step for ReHo analysis because the effects of GSR correction on ReHo are non-linear and complicated (Qing et al., 2015; Zuo et al., 2013a) and methodological variance that contributes to GSR can artifactually inflate ReHo through global autocorrelation (Kruschwitz et al., 2015; Yeo et al., 2015). The study by Li and colleagues demonstrated inclusion of GSR led to a significant improvement in the variance explained by the local rsFC in behavioral tasks in two independent datasets (Li et al., 2019). No analyses were performed to examine whether our study findings would differ without GSR, a shortcoming of the rsfMRI data processing.

This study has a few limitations. Analyses were performed in adult participants with no neuropsychiatric disorders and the FCVRS → CBF → ReHo pathway may be altered in participants with these disorders. Future analyses should be focused on the effects of FCVRS → CBF → ReHo in subjects with neuropsychiatric illnesses to understand the complex interplay between neuropsychiatric and cardiovascular illnesses on cerebral connectivity, circulation and metabolism. Mediation analyses included FCVRS as an independent variable and were also extended to the components of FCVRS. The analyses can still be extended to other measures such as low-/very low-density lipoprotein cholesterol, C-reactive protein, hematocrit, body mass index, triglycerides, etc. though they were not included as contributing factors for FCVRS and may have influences on the CBF and ReHo measurements and their relationships. Potential confounders, such as levels of physical fitness, economic status, diet and others, were not included in the mediation analysis, which may in part influence the analysis results. Since this was a cross-sectional study, establishing directional effects in the full FCVRS → CBF → ReHo pathway is challenging. This overarching hypothesis needs to be confirmed in other cohorts too. We used a longitudinal test-retest sample to demonstrate the significance of the latter part (CBF → ReHo) of the pathway, but further analyses would be needed to demonstrate the validity of the full pathway. The ACP participants had higher environmental homogeneity, and shared a traditional rural upbringing, similar educational levels, and due to strong cultural prohibitions, had low rates of use of alcohol, tobacco, and other drugs (Fuchs et al., 1990). A caution should be used in interpreting the research findings and requires assessments of the generalizability of these findings in additional populations.

In conclusion, ReHo findings are commonly interpreted as differences in localized cerebral connectivity, however, global, and regional ReHo signal show significant linkage with CBF

and both are influenced by cardiovascular risk factors in a complex and regional way. We recommend that future studies consider differences in cardiovascular health while interpreting ReHo findings. Specifically, the ReHo findings in neuropsychiatry cohorts may in part reflect differences in the underlying cardiovascular disease risk rather than specifically the differences in local connectivity. This study highlighted the complex relationship between cardiovascular and nervous systems and advanced our knowledge on the biology of the underlying ReHo signal.

## Supplementary Material

Refer to Web version on PubMed Central for supplementary material.

## Funding

Support was received from NIH grants U01MH108148, DP1DA048968, R01EB015611, and R01MH121246.

## Data Availability

Data will be made available on request.

## References

Adhikari BM, Jahanshad N, Shukla D, Glahn DC, Blangero J, Reynolds RC, Cox RW, Fieremans E, Veraart J, Novikov DS, Nichols TE, Hong LE, Thompson PM, Kochunov P, 2018a. Comparison of heritability estimates on resting state fMRI connectivity phenotypes using the ENIGMA analysis pipeline. Hum. Brain Mapp 39, 4893–4902. [PubMed: 30052318]

Adhikari BM, Jahanshad N, Shukla DK, Glahn DC, Blangero J, Reynolds RC, Cox RW, Fieremans E, Veraart J, Novikov DS, Nichols TE, Hong LE, Thompson PM, Kochunov P, 2018b. Heritability estimates on resting state fMRI data using ENIGMA analysis pipeline. Pac. Symp. Biocomput 23, 307–318. [PubMed: 29218892]

Adhikari BM, Jahanshad N, Shukla DK, Turner JA, Grotegerd D, Dannlowski U, Kugel H, Engelen J, Dietsche B, Krug A, Kircher T, Fieremans E, Veraart J, Novikov DS, Boedhoe PSW, van der Werf YD, van den Heuvel OA, Ipser J, Uhlmann A, Stein DJ, Dickie E, Voineskos AN, Malhotra AK, Pizzagalli F, Calhoun VC, Waller L, Veer IM, Walter H, Buchanan RW, Glahn DC, Hong LE, Thompson PM, Kochunov P, 2019. A resting state fMRI analysis pipeline for pooling inference across diverse cohorts: an ENIGMA rs-fMRI protocol. Brain Imaging Behav 13, 1453–1467. [PubMed: 30191514]

Albrecht D, Isenberg AL, Stradford J, Monreal T, Sagare A, Pachicano M, Sweeney M, Toga A, Zlokovic B, Chui H, Joe E, Schneider L, Conti P, Jann K, Pa J, 2020. Associations between Vascular Function and Tau PET Are Associated with Global Cognition and Amyloid. J. Neurosci 40, 8573–8586. [PubMed: 33046556]

Alfaro-Almagro F, Jenkinson M, Bangerter NK, Andersson JLR, Griffanti L, Douaud G, Sotiropoulos SN, Jbabdi S, Hernandez-Fernandez M, Vallee E, Vidaurre D, Webster M, McCarthy P, Rorden C, Daducci A, Alexander DC, Zhang H, Dragonu I, Matthews PM, Miller KL, Smith SM, 2018. Image processing and Quality Control for the first 10,000 brain imaging datasets from UK Biobank. Neuroimage 166, 400–424. [PubMed: 29079522]

Alsop DC, Detre JA, Golay X, Gunther M, Hendrikse J, Hernandez-Garcia L, Lu H, MacIntosh BJ, Parkes LM, Smits M, van Osch MJ, Wang DJ, Wong EC, Zaharchuk G, 2015. Recommended implementation of arterial spin-labeled perfusion MRI for clinical applications: a consensus of the ISMRM perfusion study group and the European consortium for ASL in dementia. Magn. Reson. Med 73, 102–116. [PubMed: 24715426]

An L, Cao QJ, Sui MQ, Sun L, Zou QH, Zang YF, Wang YF, 2013. Local synchronization and amplitude of the fluctuation of spontaneous brain activity in attention-deficit/hyperactivity disorder: a resting-state fMRI study. Neurosci. Bull 29, 603–613. [PubMed: 23861089]

Beauchet O, Celle S, Roche F, Bartha R, Montero-Odasso M, Allali G, Annweiler C, 2013. Blood pressure levels and brain volume reduction: a systematic review and meta-analysis. J. Hypertens 31, 1502–1516. [PubMed: 23811995]

Bersani FS, Mellon SH, Reyus VI, Wolkowitz OM, 2019. Accelerated aging in serious mental disorders. Curr. Opin. Psychiatry 32, 381–387. [PubMed: 31145144]

Birn RM, Diamond JB, Smith MA, Bandettini PA, 2006. Separating respiratory-variation-related fluctuations from neuronal-activity-related fluctuations in fMRI. Neuroimage 31, 1536–1548. [PubMed: 16632379]

Biswal B, Yetkin FZ, Haughton VM, Hyde JS, 1995. Functional connectivity in the motor cortex of resting human brain using echo-planar MRI. Magn. Reson. Med 34, 537–541. [PubMed: 8524021]

Blair GW, Thrippleton MJ, Shi Y, Hamilton I, Stringer M, Chappell F, Dickie DA, Andrews P, Marshall I, Doubal FN, Wardlaw JM, 2020. Intracranial hemodynamic relationships in patients with cerebral small vessel disease. Neurology 94, e2258–e2269. [PubMed: 32366534]

Briggs R, Carey D, Claffey P, McNicholas T, Newman L, Nolan H, Kennelly SP, Kenny RA, 2019. The association between frontal lobe perfusion and depressive symptoms in later life. Br. J. Psychiatry 214, 230–236. [PubMed: 30606275]

Carmichael O, 2014. Preventing vascular effects on brain injury and cognition late in life: knowns and unknowns. Neuropsychol. Rev 24, 371–387. [PubMed: 25085314]

Casey DE, Haupt DW, Newcomer JW, Henderson DC, Sernyak MJ, Davidson M, Lindenmayer J−.P., Manoukian, S.V., Banerji, M.A., Lebovitz, H.E., Hennekens, C.H., 2004. Antipsychotic-induced weight gain and metabolic abnormalities: implications for increased mortality in patients with schizophrenia. J. Clin. Psychiatry 65, 4–18.

Cavazzuti M, Porro CA, Biral GP, Benassi C, Barbieri GC, 1987. Ketamine effects on local cerebral blood flow and metabolism in the rat. J. Cereb. Blood Flow Metabol 7, 806–811.

Chappell MA, Groves AR, MacIntosh BJ, Donahue MJ, Jezzard P, Woolrich MW, 2011. Partial volume correction of multiple inversion time arterial spin labeling MRI data. Magn. Reson. Med 65, 1173–1183. [PubMed: 21337417]

Chen J, Xu Y, Zhang K, Liu Z, Xu C, Shen Y, Xu Q, 2013. Comparative study of regional homogeneity in schizophrenia and major depressive disorder. Am. J. Med. Genet. B 162B, 36–43.

Chen OY, Crainiceanu C, Ogburn EL, Caffo BS, Wager TD, Lindquist MA, 2018. High-dimensional multivariate mediation with application to neuroimaging data. Biostatistics 19, 121–136. [PubMed: 28637279]

D'Agostino RB Sr, Vasan RS, Pencina MJ, Wolf PA, Cobain M, Massaro JM, Kannel WB, 2008. General cardiovascular risk profile for use in primary care: the Framingham Heart Study. Circulation 117, 743–753. [PubMed: 18212285]

Dai Z, Yan C, Wang Z, Wang J, Xia M, Li K, Hi Y, 2012. Discriminative analysis of early Alzheimer's disease using multi-modalimaging andmulti-level characterization with multi-classifier (M3). Neuroimage 59, 2187–2195. [PubMed: 22008370]

del Valle MC, Loebel AD, Murray S, Yang R, Harrison DJ, Cuffel BJ, 2006. Change in framingham risk score in patients with schizophrenia: a post hoc analysis of a randomized, double-blind, 6-week trial of ziprasidone and olanzapine. Prim. Care Companion J. Clin. Psychiatry 8, 329–333. [PubMed: 17245453]

Detre JA, Leigh JS, Williams DS, Koretsky AP, 1992. Perfusion imaging. Magn. Reson. Med 23, 37–45. [PubMed: 1734182]

Dong Z, Liu Z, Liu Y, Zhang R, Mo H, Gao L, Shi Y, 2020. Physical exercise rectifies CUMS-induced aberrant regional homogeneity in mice accompanied by the adjustment of skeletal muscle PGC-1a/IDO1 signals and hippocampal function. Behav. Brain Res 383, 112516. [PubMed: 32006566]

Dounavi ME, Low A, McKiernan EF, Mak E, Muniz-Terrera G, Ritchie K, Ritchie CW, Su L, O'Brien JT, 2021. Evidence of cerebral hemodynamic dysregulation in middle-aged APOE *ε*4 carriers: the PREVENT-Dementia study. J. Cereb. Blood Flow Metab 41, 2844–2855. [PubMed: 34078163]

Fang X, Zhang R, Bao C, Zhou M, Yan W, Lu S, Xie S, Zhang X, 2021. Abnormal regional homogeneity (ReHo) and fractional amplitude of low frequency fluctuations (fALFF) in first-episode drug-naive schizophrenia patients comorbid with depression. Brain Imaging Behav 15, 2627–2636. [PubMed: 33788124]

Fox MD, Snyder AZ, Vincent JL, Raichle ME, 2007. Intrinsic fluctuations within cortical systems account for intertrial variability in human behavior. Neuron 56, 171–184. [PubMed: 17920023]

Fuchs JA, Levinson RM, Stoddard RR, Mullet ME, Jones DH, 1990. Health risk factors among the Amish: results of a survey. Health Educ. Q 17, 197–221. [PubMed: 2347695]

Gao S, Ming Y, Wang J, Gu Y, Ni S, Lu S, Zhang R, Sun J, Zhang N, Xu X, 2020. Enhanced prefrontal regional homogeneity and its correlations with cognitive dysfunction/psychopathology in patients with first-diagnosed and drug-Naive Schizophrenia. Front. Psychiatry 11, 580570. [PubMed: 33192722]

Giordano V, Peluso G, Iannuccelli M, Benatti P, Nicolai R, Calvani M, 2007. Systemic and brain metabolic dysfunction as a new paradigm for approaching Alzheimer's dementia. Neurochem. Res 32, 555–567. [PubMed: 16915364]

Glymour C, Zhang K, Spirtes P, 2019. Review of causal discovery methods based on graphical models. Front. Genet 10, 524. [PubMed: 31214249]

Gonzales MM, Ajilore O, Charlton RC, Cohen J, Yang S, Sieg E, Bhaumik DK, Kumar A, Lamar M, 2017. Divergent influences of cardiovascular disease risk factor domains on cognition and gray and white matter morphology. Psychosom. Med 79, 541–548. [PubMed: 28498826]

Haight TJ, Bryan RN, Erus G, Davatzikos C, Jacobs DR, D'Esposito M, Lewis CE, Launer LJ, 2015. Vascular risk factors, cerebrovascular reactivity, and the default– mode brain network. Neuroimage 115, 7–16. [PubMed: 25917517]

Han Y, Wang J, Zhao Z, Min B, Lu J, Li K, He Y, Jia J, 2011. Frequency-dependent changes in the amplitude of low-frequency fluctuations in amnestic mild cognitive impairment: a resting-state fMRI study. Neuroimage 55, 287–295. [PubMed: 21118724]

Hassoun W, Le Cavorsin M, Ginovart N, Zimmer L, Gualda V, Bonnefoi F, Leviel V, 2003. PET study of the [11C]raclopride binding in the striatum of the awake cat: effects of anaesthetics and role of cerebral blood flow. Eur. J. Nucl. Med. Mol. Imaging 30, 141–148. [PubMed: 12483422]

Holiga S, Sambataro F, Luzy C, Greig G, Sarkar N, Renken RJ, Marsman JC, Schobel SA, Bertolino A, Dukart J, 2018. Test-retest reliability of task-based and resting-state blood oxygen level dependence and cerebral blood flow measures. PLoS One 13, e0206583. [PubMed: 30408072]

Hoogenboom WS, Marder TJ, Flores VL, Huisman S, Eaton HP, Schneiderman JS, Bolo NR, Simonson DC, Jacobson AM, Kubicki M, Shenton ME, Musen G, 2014. Cerebral white matter integrity and resting-state functional connectivity in middle-aged patients with type 2 diabetes. Diabetes 63, 728–738. [PubMed: 24203723]

Iwabuchi SJ, Krishnadas R, Li C, Auer DP, Radua J, Palaniyappan L, 2015. Localized connectivity in depression: a meta-analysis of resting state functional imaging studies. Neurosci. Biobehav. Rev 51, 77–86. [PubMed: 25597656]

Jahanshad N, Lee AD, Barysheva M, McMahon KL, de Zubicaray GI, Martin NG, Wright MJ, Toga AW, Thompson PM, 2010. Genetic influences on brain asymmetry: a DTI study of 374 twins and siblings. Neuroimage 52, 455–469. [PubMed: 20430102]

Jiang L, Xu Y, Zhu XT, Yang Z, Li HJ, Zuo XN, 2015. Local to remote cortical connectivity in early and adulthood onset schizophrenia. Transl. Psychiatry 5, e566. [PubMed: 25966366]

Jiang L, Zuo XN, 2016. Regional homogeneity: a multimodal, multiscale neuroimaging marker of the human connectome. Neuroscientist 22, 486–505. [PubMed: 26170004]

Kruschwitz JD, Meyer-Lindenberg A, Veer IM, Wackerhagen C, Erk S, Mohnke S, Pohland L, Haddad L, Grimm O, Tost H, Romanczuk-Seiferth N, 2015. Segregation of face sensitive areas within the fusiform gyrus using global signal regression? A study on amygdala resting-state functional connectivity. Hum. Brain Mapp 36, 4089–4103. [PubMed: 26178527]

Knight SP, Laird E, Williamson W, O'Connor J, Newman L, Carey D, De Looze C, Fagan AJ, Chappell MA, Meaney JF, Kenny RA, 2021. Obesity is associated with reduced cerebral blood flow - modified by physical activity. Neurobiol. Aging 105, 35–47. [PubMed: 34022537]

Kuczynski B, Jagust W, Chui HC, Reed B, 2009a. An inverse association of cardiovascular risk and frontal lobe glucose metabolism. Neurology 71, 738–743.

Kuczynski B, Jagust W, Chui HC, Reed B, 2009b. An inverse association of cardiovascular risk and frontal lobe glucose metabolism. Neurology 72, 738–743. [PubMed: 19237703]

Li H, Lin Y, Chen J, Wang X, Wu Q, Li Q, Chen Z, 2017. Abnormal regional homogeneity and functional connectivity in adjustment disorder of new recruits: a resting-state fMRI study. Jpn. J. Radiol 35, 151–160. [PubMed: 28144895]

Li J, Kong R, Liegeois R, Orban C, Tan Y, Sun N, Holmes AJ, Sabuncu MR, Ge T, Yeo BTT, 2019. Global signal regression strengthens association between resting-state functional connectivity and behavior. Neuroimage 196, 126–141. [PubMed: 30974241]

Li J, Yang R, Xia K, Wang T, Nie B, Gao K, Chen J, Zhao H, Li Y, Wang W, 2018. Effects of stress on behavior and resting-state fMRI in rats and evaluation of Telmisartan therapy in a stress-induced depression model. BMC Psychiatry 18, 337. [PubMed: 30333002]

Li Z, Zhu Y, Childress AR, Detre JA, Wang Z, 2012. Relations between BOLD fMRI-derived resting brain activity and cerebral blood flow. PLoS One 7, e44556. [PubMed: 23028560]

Lim IA, Faria AV, Li X, Hsu JT, Airan RD, Mori S, van Zijl PC, 2013. Human brain atlas for automated region of interest selection in quantitative susceptibility mapping: application to determine iron content in deep gray matter structures. Neuroimage 82, 449–469. [PubMed: 23769915]

Luchsinger JA, Gustafson DR, 2009. Adiposity, type 2 diabetes, and Alzheimer's disease. J. Alzheimers Dis 16, 693–704. [PubMed: 19387106]

Meng L, Hou W, Chui J, Han R, Gelb AW, 2015. Cardiac output and cerebral blood flow: the integrated regulation of brain perfusion in adult humans. Anesthesiology 123, 1198–1208. [PubMed: 26402848]

Nichols TE, Holmes AP, 2002. Nonparametric permutation tests for functional neuroimaging: a primer with examples. Hum. Brain Mapp 15, 1–25. [PubMed: 11747097]

Nugent KL, Million-Mrkva A, Backman J, Stephens SH, Reed RM, Kochunov P, Pollin TI, Shuldiner AR, Mitchell BD, Hong LE, 2014. Familial aggregation of tobacco use behaviors among Amish men. Nicotine Tob. Res 16, 923–930. [PubMed: 24583363]

Petrides M, 2007. The orbitofrontal cortex: novelty, deviation from expectation, and memory. Ann. N. Y. Acad. Sci 1121, 33–53. [PubMed: 17872393]

Power JD, Mitra A, Laumann TO, Snyder AZ, Schlaggar BL, Petersen SE, 2014. Methods to detect, characterize, and remove motion artifact in resting state fMRI. Neuroimage 84, 320–341. [PubMed: 23994314]

Qiu C, Liao W, Ding J, Feng Y, Zhu C, Nie X, Zhang W, Chen H, Gong Q, 2011. Regional homogeneity changes in social anxiety disorder: a resting-state fMRI study. Psychiatry Res 194, 47–53. [PubMed: 21831605]

Qing Z, Dong Z, Li S, Zang Y, Liu D, 2015. Global signal regression has complex effects on regional homogeneity of resting state fMRI signal. Magnetic Resonance Imaging 33 (10), 1306–1313. [PubMed: 26234499]

Rao JS, Liu Z, Zhao C, Wei RH, Zhao W, Tian PY, Zhou X, Yang ZY, Li XG, 2017. Ketamine changes the local resting-state functional properties of anesthetized– monkey brain. Magn. Reson. Imaging 43, 144–150. [PubMed: 28755862]

Rao JS, Ma M, Zhao C, Liu Z, Yang ZY, Li XG, 2015. Alteration of brain regional homogeneity of monkeys with spinal cord injury: a longitudinal resting-state functional magnetic resonance imaging study. Magn. Reson. Imaging 33, 1156–1162. [PubMed: 26117702]

Roberts RO, Knopman DS, Przybelski SA, Mielke MM, Kantarci K, Preboske GM, Senjem ML, Pankratz VS, Geda YE, Boeve BF, Ivnik RJ, Rocca WA, Petersen RC, Jack JCR, 2014. Association of type 2 diabetes with brain atrophy and cognitive impairment. Neurology 82, 1132–1141. [PubMed: 24647028]

Serang S, Jacobucci R, Brimhall KC, Grimm KJ, 2017. Exploratory mediation analysis via regularization. Struct. Equ. Model 24, 733–744.

Sheng K, Fang W, Zhu Y, Shuai G, Zou D, Su M, Han Y, Cheng O, 2016. Different alterations of cerebral regional homogeneity in early-onset and late-onset Parkinson's disease. Front. Aging Neurosci 8, 165. [PubMed: 27462265]

Song Y, Huang C, Zhong Y, Wang X, Tao G, 2022. Abnormal reginal homogeneity in left anterior cingulum cortex and precentral gyrus as a potential neuroimaging biomarker for first-episode major depressive disorder. Front. Psychiatry 13, 924431.

Sugita T, Kondo Y, Ishino S, Mori I, Horiguchi T, Ogawa M, Magata Y., 2018. Evaluation of drug effects on cerebral blood flow and glucose uptake in un-anesthetized and un-stimulated rats: application of free-moving apparatus enabling to keep rats free during PET/SPECT tracer injection and uptake. Nucl. Med. Commun 39, 753–760. [PubMed: 29771718]

Temma T, Kuge Y, Sano K, Kamihashi J, Obokata N, Kawashima H, Magata Y, Saji H, 2008. PET O-15 cerebral blood flow and metabolism after acute stroke in spontaneously hypertensive rats. Brain Res 1212, 18–24. [PubMed: 18445493]

Timothy JR, Lambert DV, Pantelis C, 2003. Medical comorbidity in schizophrenia. Med. J. Aust 178, S67–S70. [PubMed: 12720526]

Ullsperger M, von Cramon DY, 2001. Subprocesses of performance monitoring: a dissociation of error processing and response competition revealed by event-related fMRI and ERPs. Neuroimage 14, 1387–1401. [PubMed: 11707094]

Veraart J, Novikov DS, Christiaens D, Ades-Aron B, Sijbers J, Fieremans E, 2016. Denoising of diffusion MRI using random matrix theory. Neuroimage 142, 394–406. [PubMed: 27523449]

Viron MJ, Stern TA, 2010. The impact of serious mental illness on health and healthcare. Psychosomatics 51, 458–465. [PubMed: 21051676]

Wang J, Zhang JR, Zang YF, Wu T, 2018. Consistent decreased activity in the putamen in Parkinson's disease: a meta-analysis and an independent validation of resting-state fMRI. Gigascience 7.

Wang L, Song M, Jiang T, Zhang Y, Yu C, 2011. Regional homogeneity of the resting-state brain activity correlates with individual intelligence. Neurosci. Lett 488, 275–278. [PubMed: 21108990]

Wang R, Fratiglioni L, Laukka EJ, Lovden M, Kalpouzos G, Keller L, Graff C, Salami A, Bäckman L, Qiu C, 2015. Effects of vascular risk factors and APOE epsilon4 on white matter integrity and cognitive decline. Neurology 84, 1128–1135. [PubMed: 25672924]

Wang S, Wang G, Lv H, Wu R, Zhao J, Guo W, 2016. Abnormal regional homogeneity as potential imaging biomarker for psychosis risk syndrome: a resting-state fMRI study and support vector machine analysis. Sci. Rep 6, 27619. [PubMed: 27272341]

Wertz J, Caspi A, Ambler A, Broadbent J, Hancox RJ, Harrington H, Hogan S, Houts RM, Leung JH, Poulton R, Purdy SC, Ramrakha S, Rasmussen LJH, Richmond-Rakerd LS, Thorne PR, Wilson GA, Moffitt TE, 2021. Association of history of psychopathology with accelerated aging at midlife. JAMA Psychiatry 78, 530–539. [PubMed: 33595619]

Williams DS, Detre JA, Leigh JS, Koretsky AP, 1992. Magnetic resonance imaging of perfusion using spin inversion of arterial water. Proc. Natl. Acad. Sci. U. S. A. 89, 212–216. [PubMed: 1729691]

Williams LR, Leggett RW, 1989. Reference values for resting blood flow to organs of man. Clin. Phys. Physiol. Meas. 10, 187–217. [PubMed: 2697487]

Wu Q, Huang X, Culbreth A, Waltz J, Hong LE, Chen S, 2020. Extracting brain disease-related connectome subgraphs by adaptive dense subgraph discovery. bioRxiv.

Wu T, Grandjean J, Bosshard SC, Rudin M, Reutens D, Jiang T, 2017. Altered regional connectivity reflecting effects of different anaesthesia protocols in the mouse brain. Neuroimage 149, 190–199. [PubMed: 28159688]

Xiao B, Wang S, Liu J, Meng T, He Y, Luo X, 2017. Abnormalities of localized connectivity in schizophrenia patients and their unaffected relatives: a meta-analysis of resting-state functional magnetic resonance imaging studies. Neuropsychiatr. Dis. Treat 13, 467. [PubMed: 28243099]

Xu Y, Zhuo C, Qin W, Zhu J, Yu C, 2015. Altered spontaneous brain activity in schizophrenia: a meta-analysis and a large-sample study. Biomed. Res. Int 2015, 204628. [PubMed: 26180786]

Yan H, Shan X, Li H, Liu F, Guo W, 2022. Abnormal spontaneous neural activity in hippocampal–cortical system of patients with obsessive–compulsive disorder and its potential for diagnosis and prediction of early treatment response. Front. Cell Neurosci 16.

Yeo BT, Tandi J, Chee MW, 2015. Functional connectivity during rested wakefulness predicts vulnerability to sleep deprivation Neuroimage 26 (111), 147–158.

Zang Y, Jiang T, Lu Y, He Y, Tian L, 2004. Regional homogeneity approach to fMRI data analysis. Neuroimage 22, 394–400. [PubMed: 15110032]

Zhang Z, Liu Y, Jiang T, Zhou B, An N, Dai H, Wang P, Niu Y, Wang L, Zhang X, 2012. Altered spontaneous activity in Alzheimer's disease and mild cognitive impairment revealed by Regional Homogeneity. Neuroimage 59, 1429– 1440. [PubMed: 21907292]

Zhu J, Jin Y, Wang K, Zhou Y, Feng Y, Yu M, Jin X, 2015. Frequency-dependent changes in the regional amplitude and synchronization of resting-state functional MRI in stroke. PLoS One 10, e0123850. [PubMed: 25885897]

Zhu J, Zhuo C, Xu L, Liu F, Qin W, Yu C, 2017. Altered coupling between resting-state cerebral blood flow and functional connectivity in schizophrenia. Schizophr. Bull 43, 1363–1374. [PubMed: 28521048]

Zuo XN, Xu T, Jiang L, Yang Z, Cao XY, He Y, Zang YF, Castellanos FX, Milham MP, 2013. Toward reliable characterization of functional homogeneity in the human brain: preprocessing, scan duration, imaging resolution and computational space. Neuroimage 65, 374–386. [PubMed: 23085497]

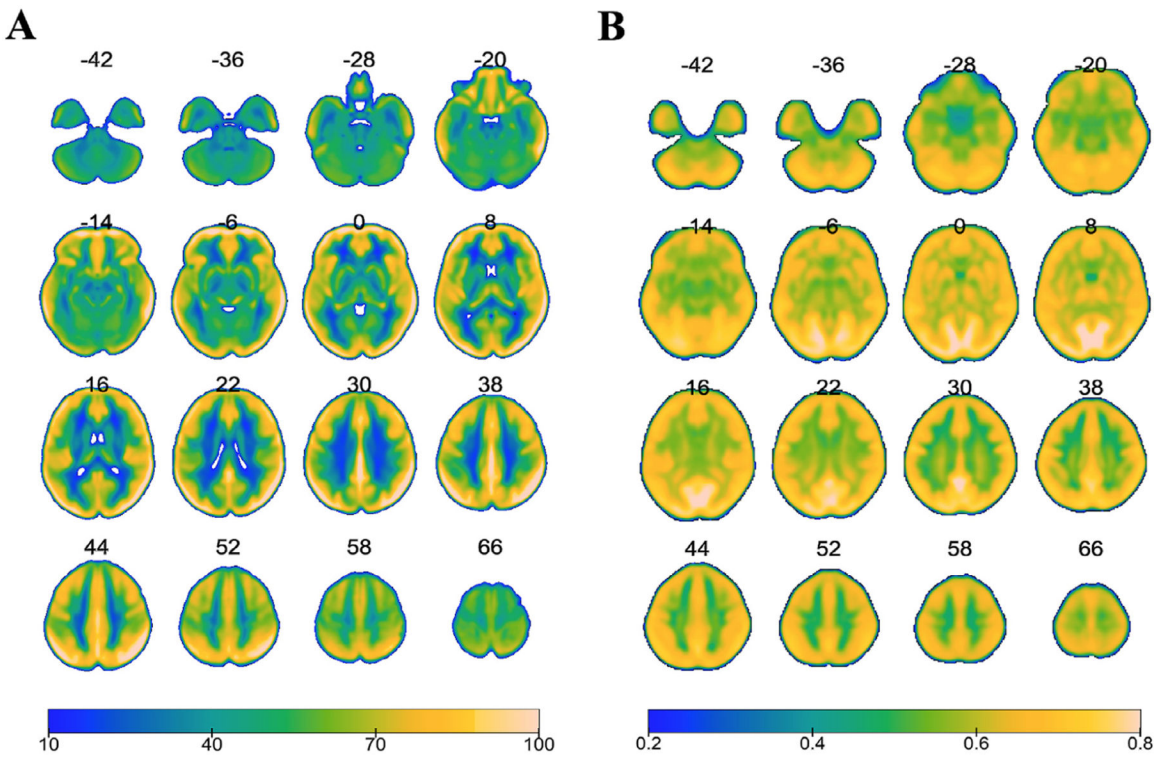


**Fig. 1.**

Average cerebral blood flow (CBF) map (**A**) and regional homogeneity (ReHo) map (**B**) in $N = 204$ participants. Numbers in the images are the z-coordinate of the axial slices. The scale for CBF ranges from 10 to 100 (mL/100 g/min); the scale for ReHo ranges from 0.2 to 0.8.

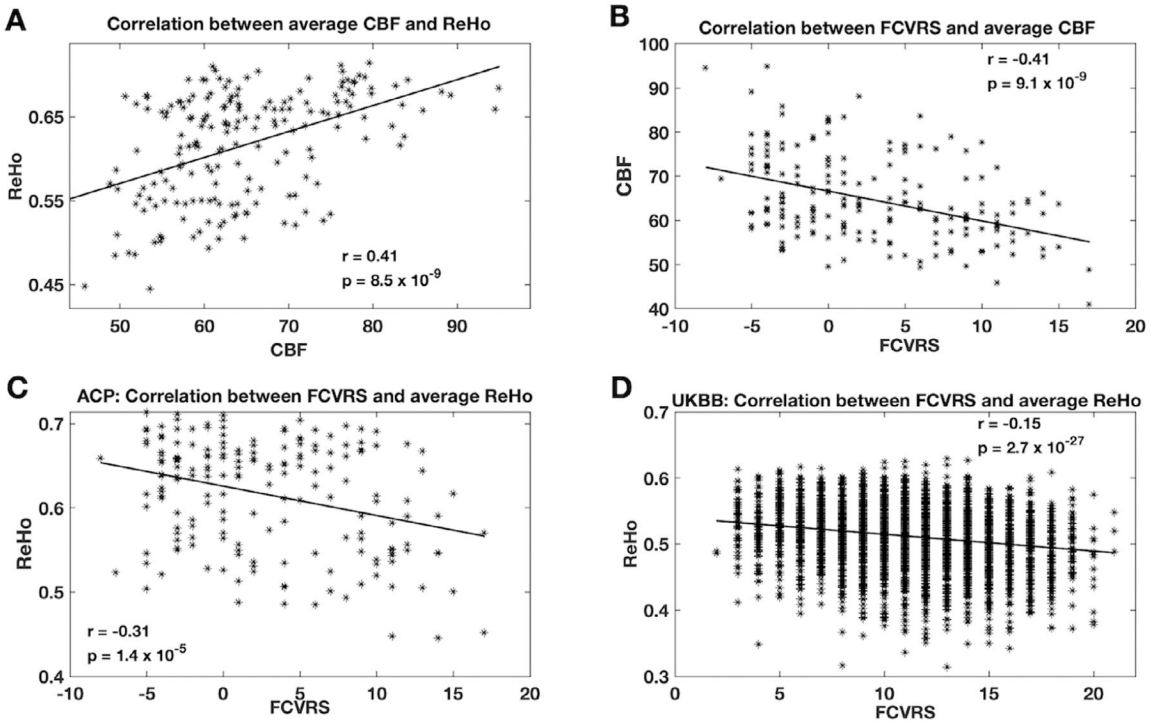


**Fig. 2. Correlations among FCVRS, CBF, and ReHo across samples.**

Data are from the Amish Connectome Project (ACP) sample unless specified otherwise. **A.** The whole-brain average cerebral blood flow (CBF) signal and regional homogeneity (ReHo) showed a significant positive correlation. **B.** Framingham cardiovascular risk score (FCVRS) showed a significantly negative correlation with the whole-brain average ReHo. **C** & **D.** FCVRS showed significant correlations with whole brain average CBF in ACP and UKBB samples, respectively. All the results presented in the figure are corrected for participants' age and sex.

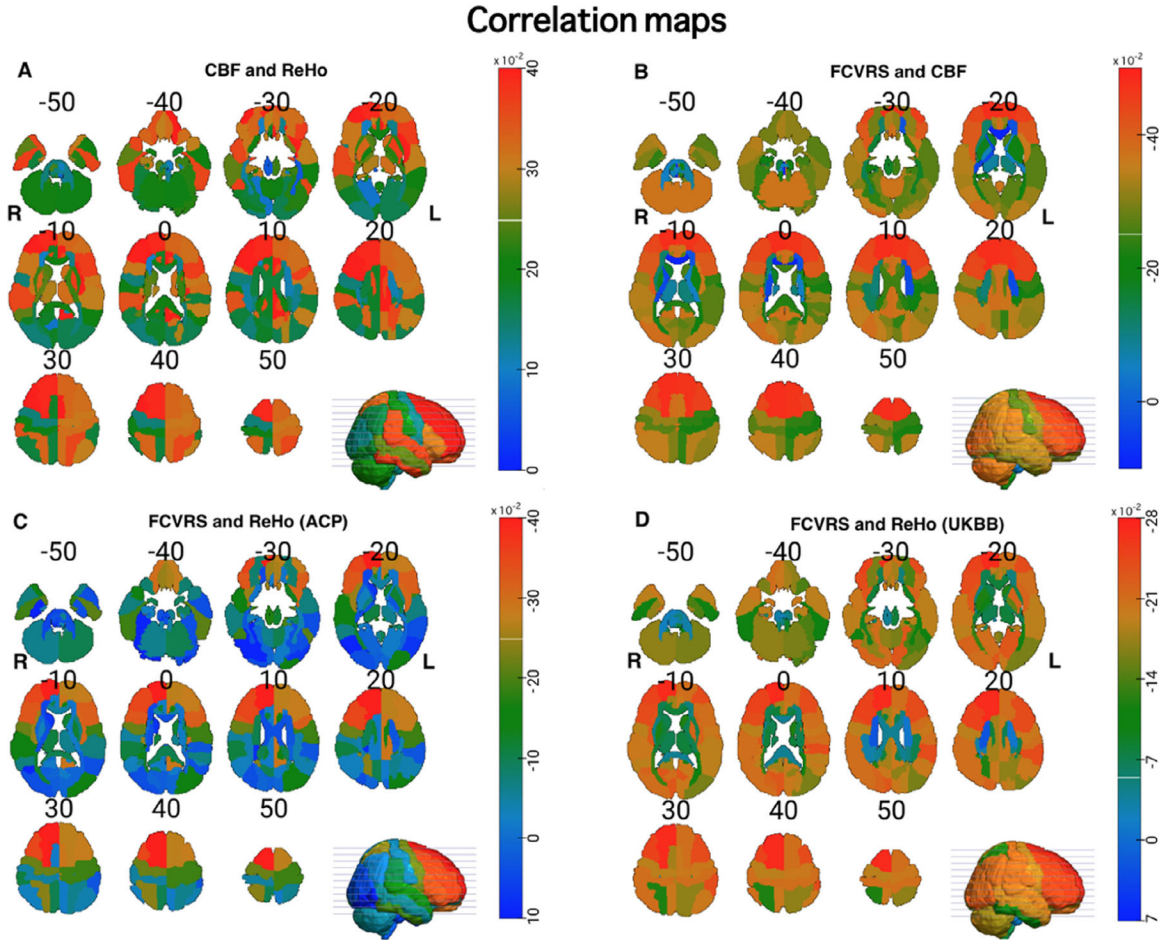


**Fig. 3. The regional correlation maps.**

Region-by-region CBF and ReHo signals were from the parcellated brain regions using JHU-MNI atlas. **A**. Whole brain CBF and ReHo correlation map, where correlation analyses were performed between regional CBF and ReHo signals from the same brain region. **B**. The Framingham cardiovascular risk score (FCVRS) and regional CBF correlation map. **C** & **D**. FCVRS score and ReHo correlation maps in ACP ($N = 204$) and UKBB ($N = 6285$) participants, respectively. Each subplot was supplied with a colorbar, and a white horizontal mark represents the color that corresponds to corrected $p < 0.05$ (multiple comparison corrections). Values in the images are the $z$-coordinates of the displayed axial slices. Positive correlations have positive $r$ values and negative correlations have negative $r$ values. Note that for B, C, and D stronger correlations were more negative. The displayed images are in radiological convention.

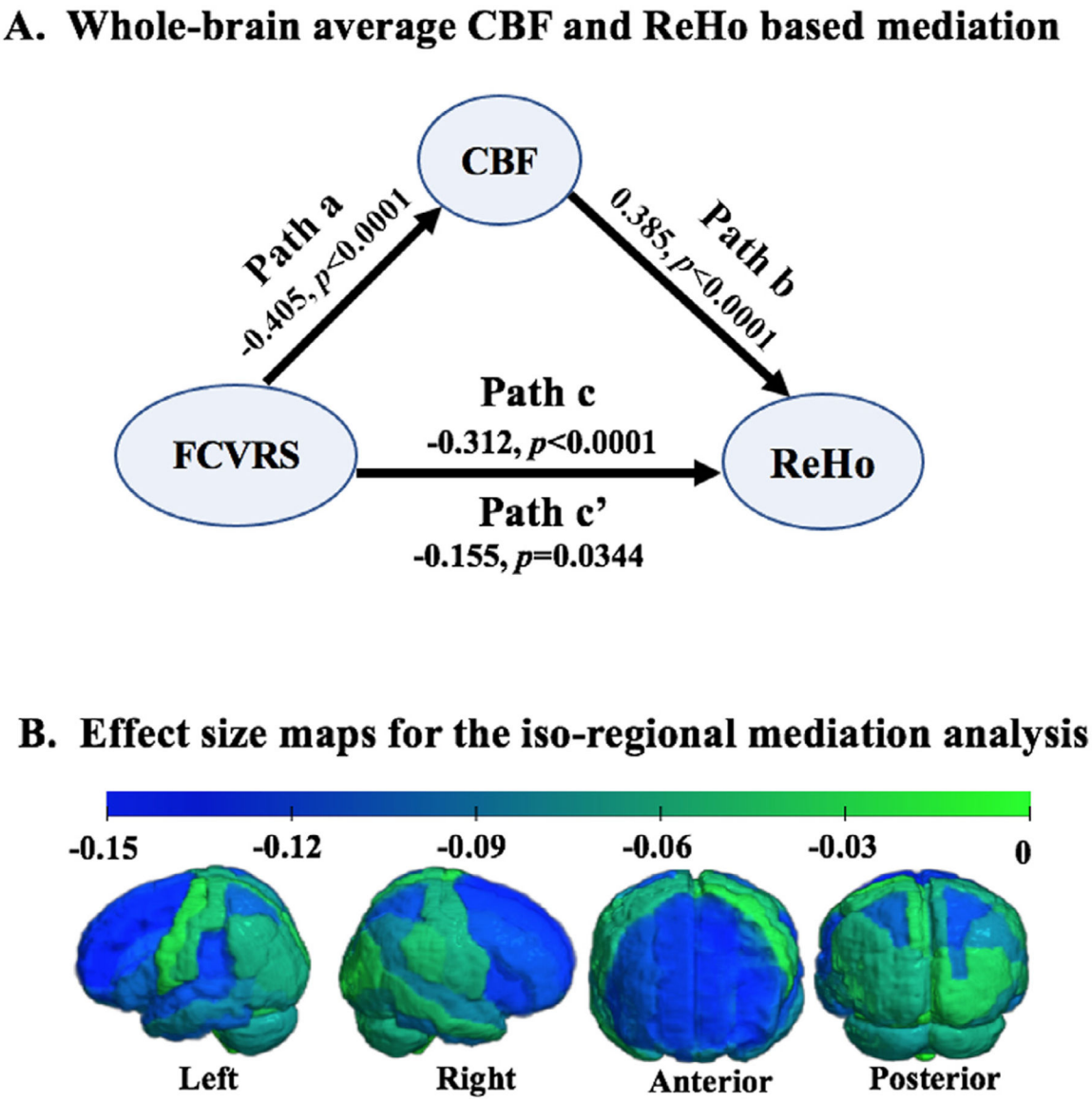


**Fig. 4. A schematic diagram of the mediation path.**

(A) Whole-brain average mediation analysis. The mediation proportion effect of FCVRS on the average ReHo through average CBF was found to be 52% ($p$<0.0001). All the requirements for a mediation effect are satisfied: Path a, b, and c are significant, and c' is significantly smaller than *c*. Path a and b together represent the indirect (mediated) effect. Path c is the direct effect and c' is the remaining direct effect of FCVRS on the average ReHo after controlling for mediating effect. (**B**) The isoregional mediation analysis involved the mediation pathway, FCVRS → a CBF region → ReHo at the same region. The strength of the mediations was mapped. Bilateral frontal and parietal areas showed the strongest effect sizes for mediation.

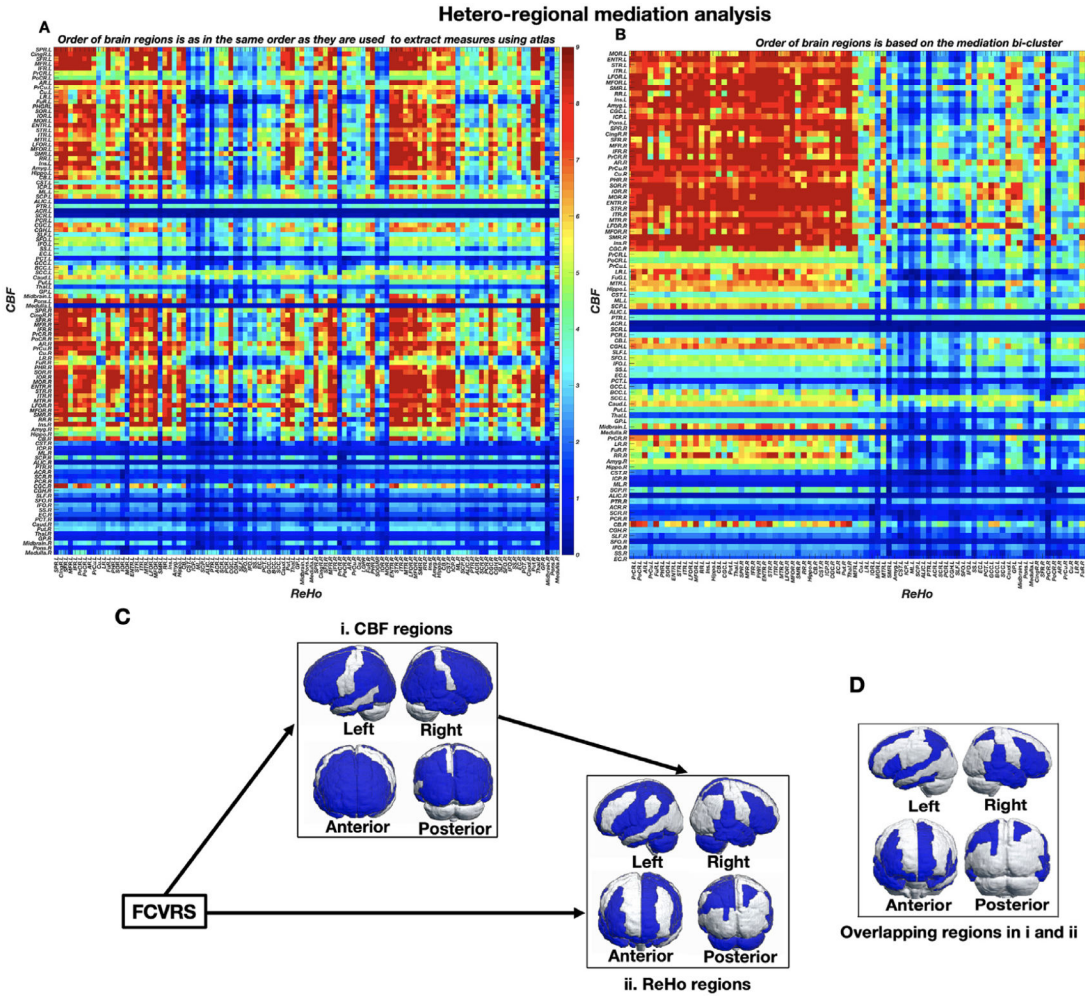


**Fig. 5. Hetero-regional mediation analysis results.**

**A**. 107×107 potential mediation pathways. Correspondingly, 107×107 *p*-values were calculated to assess the significance of the mediation effects, shown as a heatmap of -log(*p*) values. The order of CBF (y axis) and ReHo (x axis) regions is in the same order as they are used to extract CBF and ReHo measures using atlas. Full names of the abbreviations are in supplementary Table 1. B. The mediation pattern detection algorithm identified a set of CBF regions that can impact a number of ReHo regions ($p<0.0001$), re-ordered based on the mediation bi-cluster. C. (i). The CBF regions forming a cluster based on orthogonal component analysis that significantly mediated another cluster of ReHo measurements. The ReHo regions mediated by the CBF regions in (**i**) are shown in (**ii**). This hetero-regional analysis-based mediation explained about 82% of the FCVRS direct effect on the ReHo signals in the regions shown in (**ii**). **D**. The 26 regions that overlap between the 45 CBF regions and the 43 ReHo regions.